A peptide inhibitor of HIV-1 assembly *in vitro*

Jana Sticht[1], Michael Humbert[2], Stuart Findlow[3], Jochen Bodem[1], Barbara Müller[1], Ursula Dietrich[2], Jörn Werner[3] & Hans-Georg Kräusslich[1]

Formation of infectious HIV-1 involves assembly of Gag polyproteins into immature particles and subsequent assembly of mature capsids after proteolytic disassembly of the Gag shell. We report a 12-mer peptide, capsid assembly inhibitor (CAI), that binds the capsid (CA) domain of Gag and inhibits assembly of immature- and mature-like capsid particles *in vitro*. CAI was identified by phage display screening among a group of peptides with similar sequences that bind to a single reactive site in CA. Its binding site was mapped to CA residues 169–191, with an additional contribution from the last helix of CA. This result was confirmed by a separate X-ray structure analysis showing that CAI inserts into a conserved hydrophobic groove and alters the CA dimer interface. The CAI binding site is a new target for antiviral development, and CAI is the first known inhibitor directed against assembly of immature HIV-1.

Current therapy for HIV-infected patients involves a combination of inhibitors of the viral enzymes reverse transcriptase and protease, sometimes together with inhibitors of viral entry. Although combination therapy has been highly successful, its long-term efficacy is severely jeopardized by the emergence of drug-resistant variants of HIV. Accordingly, identification of alternative targets is of highest priority. Virus assembly is a particularly attractive candidate for antiviral intervention because viral structures are formed by multiple, relatively weak noncovalent interactions. However, few assembly inhibitors have been identified to date in any viral system, mainly because of insufficient information regarding particle structure and intersubunit interactions and the lack of suitable assays.

HIV is released from the infected cell as an immature, noninfectious particle containing a spherical protein shell of approximately 5,000 Gag molecules[1] underneath the viral membrane. Concomitant with release, proteolytic processing of Gag by the viral protease is initiated, leading to formation of a mature infectious virus with a conical capsid. Five sequential cleavages separate the matrix (MA), capsid (CA), nucleocapsid (NC) and p6 domains and the spacer peptides SP1 and SP2 (ref. 2) (**Fig. 1a**). In the mature virus, MA remains as a spherical layer attached to the membrane, whereas CA forms the characteristic capsid structure encasing the NC–RNA complex. Maturation proceeds by disassembly of the immature Gag shell followed by a second assembly step[1,3] that occurs inside the virion and leads to formation of the mature viral capsid. This second assembly requires the final cleavage of Gag, separating CA from the adjacent SP1 (ref. 2,4).
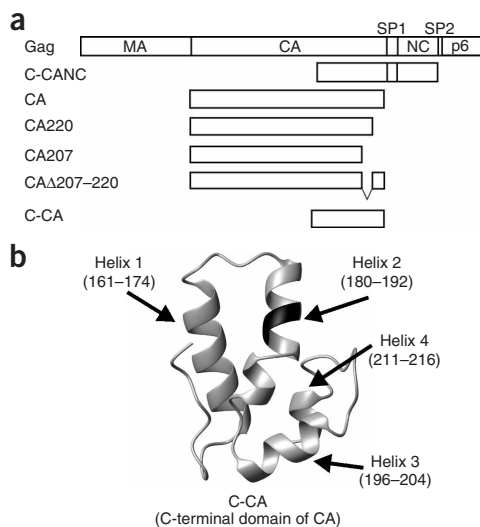
Assembly of both the immature Gag shell and the mature capsid are dependent on CA, emphasizing the structural flexibility of this Gag domain. Only limited information is currently available regarding

protein interactions driving the two assembly steps. Structure determination of CA fragments[5–8] has indicated that the N- and C-terminal regions of CA (N-CA and C-CA) represent individually folded subdomains connected by a flexible linker. Image reconstruction of *in vitro*–assembled mature capsid-like particles[9] has revealed that CA is organized in hexameric rings stabilized by interactions in helices 1–3 of N-CA[8,9] and linked to each other via the dimer interface of C-CA[9]. In solution, CA forms a dimer ($K_d = 18$ μM) whose crystallographic interface has been mapped to helix 2 of C-CA (**Fig. 1b**). Residues Trp184 and Trp185 form the center of this interface[6], which is stabilized by additional weak interactions[10]. Recent hydrogen exchange experiments provided evidence for N-CA–C-CA intersubunit interactions in the mature virus, but not in the immature virus[3,11]. The importance of these regions for mature capsid assembly has been supported by mutational analyses[12,13]. Immature capsid-like particles closely resembling the Gag shell can be assembled *in vitro*[14,15], but much less is known regarding relevant interactions in this case. Recently, it has been suggested that C-CA subdomains are exchanged between two Gag molecules during assembly of the immature shell to form a so-called swapped dimer[16], but this model awaits experimental proof.

Previous attempts to develop assembly inhibitors by targeting HIV Gag interfaces have used Gag-derived peptides[17–19], but little is known about their mechanism of action. Recently, two small molecules have been described that interfere with HIV maturation. The first, CAP-1, binds to N-CA with low affinity ($K_d \sim 800$ μM) and abolishes mature cone formation but does not interfere with virus release[20]. The second, PA-457, prevents cleavage of the CA-SP1 site[21,22] and thereby blocks assembly of the mature capsid. However, no small molecule that interferes with assembly of immature HIV particles has been described. We performed a phage display screen for peptides that

Figure 1 Illustration of Gag-derived proteins. (**a**) Schematic representation of Gag-derived proteins used. (**b**) Ribbon diagram of the structure of the C-terminal domain of CA (ref. 6), generated with MOLMOL[44]. The boundaries of helices 1–4 are indicated. The dimer interface residues Trp184 and Met185 are colored black. The orientation of the structure was chosen to best visualize the dimer interface.

Group 1 comprises all sequences selected using CA as the target protein and most sequences selected using C-CANC as the target protein; these sequences were chosen for further analysis. All group 1 peptides had substantial sequence similarity (**Table 1**).

Peptides compete with phages for CA binding

Three selected peptides were synthesized and their ability to compete with peptide-presenting phages for binding to CA was determined. CAI, the peptide most commonly selected with C-CANC (Pep1, **Table 1**), was chosen for further analysis. The peptide most commonly selected with CA (Pep2, **Table 1**, first sequence) and a peptide classified in group 4 (Pep3, **Table 1**, fourth sequence) were analyzed in parallel. CA binding of phages presenting the CAI sequence (phage-CAI) was measured in the presence of increasing peptide concentrations and normalized against binding in the absence of peptides (100%). Addition of increasing concentrations of either of the two group 1 peptides, CAI or Pep2, reduced phage binding to less than 20%, whereas Pep3 had no effect (**Fig. 2a**). Thus, both CAI and Pep2 competed with phage-CAI for binding to CA. Furthermore, CAI

bind tightly and specifically to CA and inhibit assembly. The interaction of a CA-derived protein with a selected peptide that efficiently blocked immature and mature particle assembly *in vitro* was analyzed by NMR spectroscopy, revealing the interaction site in solution and allowing the K_d of the complex to be calculated. The accompanying paper describes the crystal structure of the complex[23]. Taken together, these results show that the CAI inhibitor binds to a reactive hydrophobic pocket in CA that seems to be a promising target for antiviral drug development.

RESULTS

Phage display screening

A phage display biopanning reaction was performed on two proteins derived from HIV-1 Gag. Full-length CA (**Fig. 1a**) was used because it is the major determinant of particle assembly. The protein C-CANC, which comprises the C-CA region, SP1 and NC (**Fig. 1a**), was used because the CA-SP1 junction has been shown to be essential for assembly of immature particles[4,14,24]. NC and bovine serum albumin (BSA) were used for negative selection to increase specificity and to screen out peptides that target the nucleic acid–binding domain. Pure proteins were screened with a library of M13-derived phages presenting random 12-mer peptides at the N terminus of their pIII coat protein. After three positive and two negative selections, phage pools with a titer of 1.2×10^7 PFU μl^{-1} (CA selection) and 3.2×10^6 PFU μl^{-1} (C-CANC selection) were obtained.

After selection, specifically bound phages were detected by ELISA using an antibody to M13. In the selection for CA binding, 36 of 41 analyzed phages bound to CA but not to BSA (data not shown). The peptide-coding regions from 29 of the 36 specifically bound phages were sequenced and found to code for only two different peptides (**Table 1**). In the selection for C-CANC binding, wild-type M13 and all selected phages bound nonspecifically both to the NC domain of C-CANC and to NC. This seems to be an inherent property of M13 phages. Therefore, we tested 64 phages of the same C-CANC–selected pool for specific binding using plates coated with CA or BSA. Of these, 57 specifically interacted with CA (data not shown). The peptide-coding regions from 46 of these were sequenced and shown to code for 16 different peptides (**Table 1**). Notably, one sequence was selected multiple times when either C-CANC or CA was used as the target protein (**Table 1**, fourth sequence). Peptides were classified into four distinct groups on the basis of multiple sequence alignment (**Table 1**).

Table 1 Selected peptide sequences (by group) and peptides synthesized for further analysis

		Times selected[a]	
	Sequence	C-CANC	CA
Group 1	**IT**F**EDL**LD**YY**GP[b]	15	–
	ISW**SELD**A**FM**QM	6	–
	ISW**MDL**TA**YY**RG	–	2
	VSY**SEL**TS**YY**MR[b]	6	27
	VKY**HDL**QT**FF**DP	1	–
	VTY**AQL**QA**YF**PD	1	–
	LEF**SDL**ED**FF**RA	1	–
	LNF**SDL**NN**YF**LL	1	–
Group 2	YNEPWWLTPSMF	3	–
	LDYPWWLSMNNI	1	–
Group 3	STTWQDFFKTFG	5	–
	SYTQWDNAPGTR	1	–
Group 4	IADRPRAWIGSP[b]	1	–
	AMKTHTAIAPRA	1	–
Others	HPQMHATPYQTT	1	–
	SPSNLYEQLLHW	1	–
	LPMIDIYRTAEL	1	–

Synthetic peptides	
CAI (Pep1)[b]	ITFEDLLDYYGP
CAIctrl[c]	IYDPTLYGLEFD
Pep2[b]	VSYSELTSYYMR
Pep3[b]	IADRPRAWIGSP

[a]Numbers indicate how often sequences were selected using either C-CANC or CA as the target protein. (Phages were amplified through consecutive rounds of positive and negative selection, so selection of sequences multiple times could be the result of amplification or independent selection.) Alignment of sequences was performed using ClustalW. [b]Peptide 1 (CAI) and peptides 2 and 3 were synthesized based on selected sequences. [c]The control peptide CAIctrl has the same amino acid composition as CAI but a scrambled sequence.
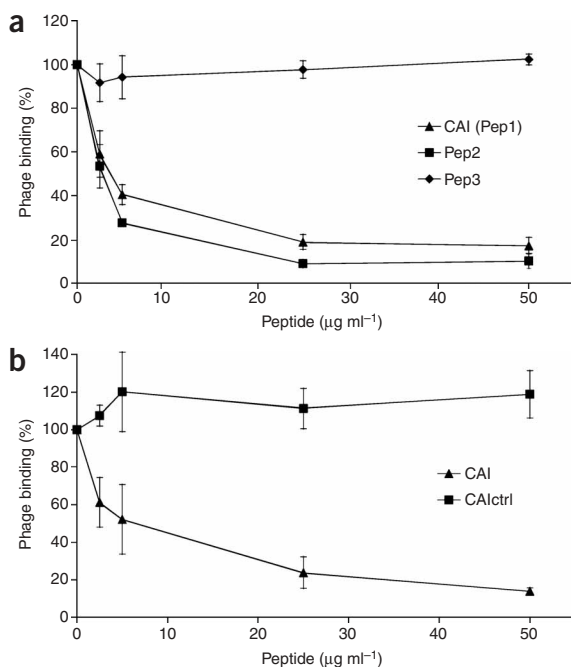
Figure 2 Results of ELISAs showing peptide competition for phage-CAI binding to CA. (**a**) Phage-CAI binding to CA in the presence of increasing concentrations of the cognate peptide CAI (Pep1), a peptide with a similar sequence (Pep2) and an unrelated peptide (Pep3). (**b**) Phage-CAI binding to CA in the presence of increasing concentrations of CAI and a peptide with a scrambled sequence (CAIctrl).

particles was reduced at a 1:2 peptide/protein ratio and was abolished at equimolar concentrations of CAI, whereas addition of a five-fold molar excess of CAIctrl had no effect (**Fig. 4a**). Because aggregation of tubes prevented counting of single particles, assemblies were pelleted by centrifugation and the amount of protein present in the resuspended pellets was analyzed by SDS-PAGE. This confirmed that assembly of CANC into tubular particles was abolished at equimolar concentrations of CAI (**Fig. 4b**). We also analyzed the effect of CAI on the *in vitro* assembly of CA, which is independent of nucleic acid but requires high protein concentrations[25]. Accordingly, high peptide concentrations were needed and the relatively high concentrations of the solvent dimethyl sulfoxide impaired the efficiency and quality of tube assembly. Despite these technical difficulties, assembly of CA was again found to be abolished by addition of CAI (data not shown). We therefore conclude that CAI inhibits *in vitro* assembly of spherical and tubular particles with similar efficiency.

Two regions within C-CA are important for CAI binding

To map the CAI binding site, the affinity of phage-CAI for CA and derivatives was compared by ELISAs (**Fig. 5**). Eight CA variants, CA220, CA207, CAΔ207–220, C-CA, CA$_{P207A}$, CA$_{E212A}$, CA$_{Q219A}$ and C-CA$_{W184A/M185A}$ (**Fig. 1a**; mutants not shown), were tested. Deletion of the last 11 flexible amino acids of CA (221–231, in CA220) had no effect on phage binding. In contrast, CA proteins lacking amino acids 207–220 (including helix 4) of C-CA showed substantially lower phage-CAI binding, as indicated by results for CA207 and CAΔ207–220. Three independent point mutations affecting the surface-exposed amino acids within helix 4 and adjacent to it (CA$_{P207A}$, CA$_{E212A}$, CA$_{Q219A}$) had no major effects, however. Thus, either

competed for CA binding with all phages presenting group 1 peptides (data not shown), indicating that all group 1 peptides target the same site. This site seems to be located in the C-CA domain, as some group 1 peptides were selected with C-CANC. Owing to limited solubility of Pep2, we focused on CAI for further analysis. Specificity of binding was demonstrated using a peptide with the same amino acid composition as CAI but with a scrambled sequence (CAIctrl). This peptide did not compete with phage-CAI for binding to CA, whereas CAI efficiently inhibited such binding (**Fig. 2b**). Thus, CAI binds efficiently and specifically to the C-CA domain.

CAI inhibits assembly *in vitro*

The ability of CAI to inhibit assembly *in vitro* was investigated by testing its influence on the formation of spherical or tubular particles from purified HIV-1 Gag–derived proteins. *In vitro* assembly of immature-like, spherical particles was performed using a recombinant Gag-derived protein lacking p6 and residues 16–99 of MA (ΔMACANCSP2) as previously described[14]. Reactions were performed with or without a five-fold molar excess of CAI or CAIctrl. In electron micrographs of negatively stained particles, formation of spherical particles was easily seen after incubation of ΔMACANCSP2 in the absence of peptide or with a five-fold molar excess of CAIctrl, but was completely abolished in the presence of a five-fold molar excess of CAI (**Fig. 3a**). Inhibition by CAI was quantified in a titration experiment. At equimolar concentrations of ΔMACANCSP2 and CAI, the number of spherical particles was about 80% lower than in the absence of CAI (**Fig. 3b**). Thus, CAI efficiently inhibits assembly of immature-like particles *in vitro*.

Mature-like tubular particles can be assembled from either CANC or CA *in vitro*[25], and their structures resemble the arrangement of CA in the conical capsid[9,26]. Assembly reactions were performed with CANC in the presence of up to a five-fold molar excess of CAI or CAIctrl. Electron micrographs of negatively stained particles at relatively low magnification were used to visualize decreasing particle numbers (**Fig. 4a**), and the integrity of tubular particles is shown at high magnification (**Fig. 4a**, insets). Assembly of CANC into tubular
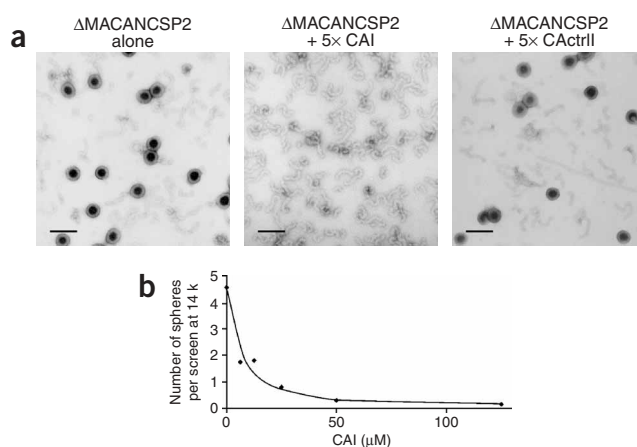

Figure 3 Inhibition of assembly of immature-like particles *in vitro*. (**a**) Negatively stained EM images of particles resulting from ΔMACANCSP2 *in vitro* assembly reactions in the absence or presence of a five-fold molar excess of CAI or CAIctrl (scale bar: 200 nm). (**b**) Concentration dependence of ΔMACANCSP2 assembly inhibition. The number of spherical particles (average of 20 viewing areas) counted on the EM screen is plotted against the concentration of CAI added to the assembly reaction (molar ratio of peptide to protein 0.25–5).
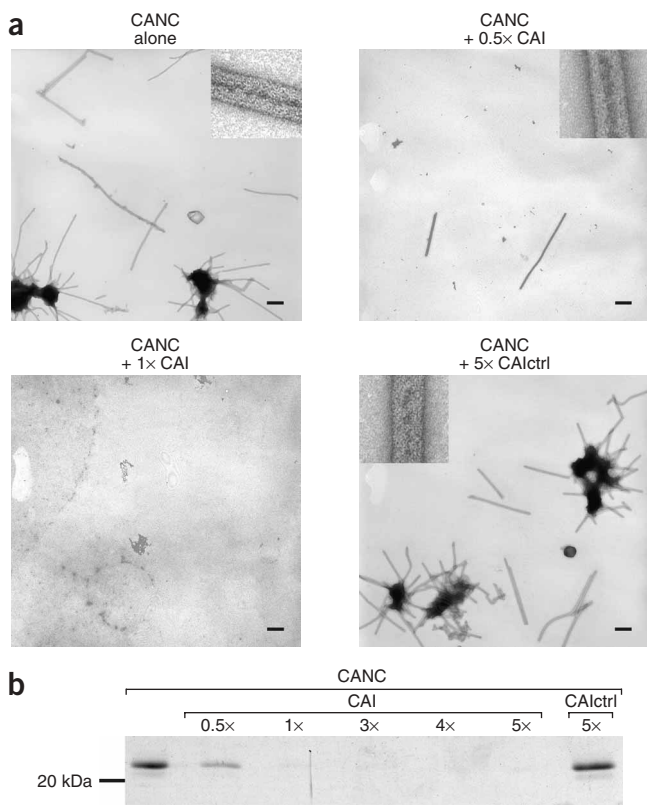
Figure 4 Inhibition of assembly of mature-like particles *in vitro*. (**a**) Negatively stained EM images of particles resulting from CANC *in vitro* assembly reactions in the absence or presence of CAI or CAIctrl (scale bar: 300 nm). Integrity of tubular particles is shown in high-magnification insets. (**b**) SDS-PAGE of pelleted particles assembled in the absence or presence of CAI or CAIctrl, showing inhibition efficiency. A molecular weight marker (in kDa) is shown on the left.

fitting. In a separate set of ^{1}H-^{15}N–HSQC experiments, a four-fold molar excess of the control peptide CAIctrl did not induce chemical shift perturbation (data not shown).

Backbone resonance assignments were obtained for the free and peptide-bound forms of C-CA$_{W184A/M185A}$. The largest chemical shift perturbations occurred within residues 169–191 (**Fig. 6b**), suggesting that this region contains the CAI binding site. The integrity of the secondary structure of CAI-bound C-CA$_{W184A/M185A}$ was confirmed by ^{13}Cα chemical shift analysis (data not shown). To allow the binding site to be visualized, residues with chemical shift perturbations larger than 0.6 p.p.m. were highlighted in red in the X-ray structure of C-CA[6] (**Fig. 6c**). This indicates that the last two turns of helix 1, the interhelical linker and helix 2 are strongly affected by peptide binding. No significant chemical shift perturbation was observed for the backbone-NH resonances of residues 207–220.

These experiments identified a binding site (CA residues 169–191) and a dissociation constant ($K_d = 15.0 \pm 7.2$ μM) for the interaction of CAI with C-CA$_{W184A/M185A}$. Because the postulated binding site contained the dimer interface residues Trp184 and Met185, and mutation of these residues had been shown to reduce the affinity of CAI for C-CA, we analyzed whether CAI binding interferes with C-CA dimerization by determining the rotational correlation times of C-CA and the C-CA–CAI complex. Because the correlation time of the dimer is about twice that of the monomer, the apparent correlation time can be used to estimate the dimerization equilibrium constant. If CAI binding disrupts the C-CA dimer, the correlation time should be lower than for CAI-free, dimeric C-CA, whereas it should be higher if CAI binding does not affect dimerization. The rotational correlation time of free C-CA at a concentration of 0.1–1 mM was 8.7–9.8 ns, consistent with the expected value for the C-CA dimerization equilibrium ($K_d \sim 18$ μM)[6]. In the presence of CAI at >95% saturation, the correlation time increased by ∼1 ns, consistent with an increased molecular weight caused by the bound peptide. Thus, CAI binding
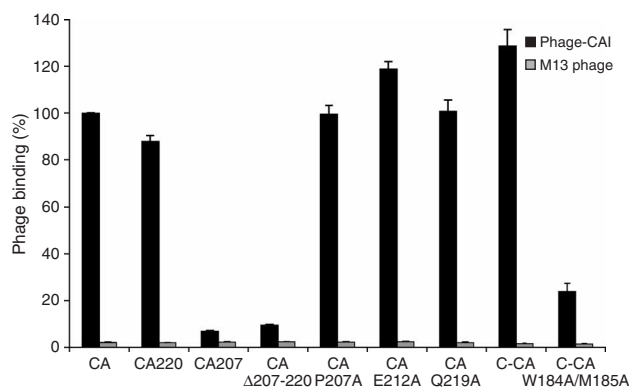
different residues are involved in the interaction, or deletion of helix 4 of C-CA induces structural rearrangements that prevent CAI binding to another site of the protein. Binding of phage-CAI to C-CA and to full-length CA was comparable, whereas the dimerization-defective protein C-CA$_{W184A/M185A}$ bound markedly less well (**Fig. 5**). Thus, either the side chains of residues Trp184 and Met185 are part of the CAI binding site, or lack of dimerization reduces the binding affinity of CAI for another site of the protein. Taken together, these results indicate that the integrity of the dimer interface and of helix 4 of C-CA are important for the interaction of CA with CAI.

CAI binds to helices 1 and 2 of C-CA

NMR chemical shift perturbation was used to further localize the binding site. Because CAI binds to the independently folded C-terminal domain of CA, we decided to use C-CA (amino acids 146–231 of CA; **Fig. 1**) for NMR analysis. We circumvented previously described problems associated with C-CA dimerization[27] by using the dimerization-defective variant C-CA$_{W184A/M185A}$. CA derivatives with these mutations have been used in several previous analyses[6,11–13,28,29], which showed that residues Trp184 and Met185 are important but not essential for particle assembly. Formation of complexes of CAI and C-CA$_{W184A/M185A}$ was clearly detectable by NMR, as indicated by chemical shift perturbation induced by peptide addition. This accords with the finding that the affinity of CAI for the mutant protein was reduced but not abolished in ELISAs (**Fig. 5**). Overlaying a series of 2D ^{1}H-^{15}N–hetero single quantum coherence (HSQC) spectra obtained for C-CA$_{W184A/M185A}$ in the absence or presence of increasing concentrations of CAI (**Fig. 6a**) shows that most peaks were unaffected (examples are circled). Yet substantial chemical shift perturbation was detectable for a subset of peaks (examples are illustrated by arrows), indicating their involvement in peptide binding. The K_d of the interaction was determined to be 15.0 ± 7.2 μM by fractional-shift

Figure 5 Results of ELISAs to detect binding of phage-CAI to various CA-derived proteins, including C-terminally truncated proteins (CA220, CA207), a deletion mutant (CAΔ207–220), variants with point mutations (CA$_{P207A}$, CA$_{E212A}$, CA$_{Q129A}$) and both the C-terminal domain of CA (C-CA) and its dimerization-defective variant (C-CA$_{W184A/M185A}$).
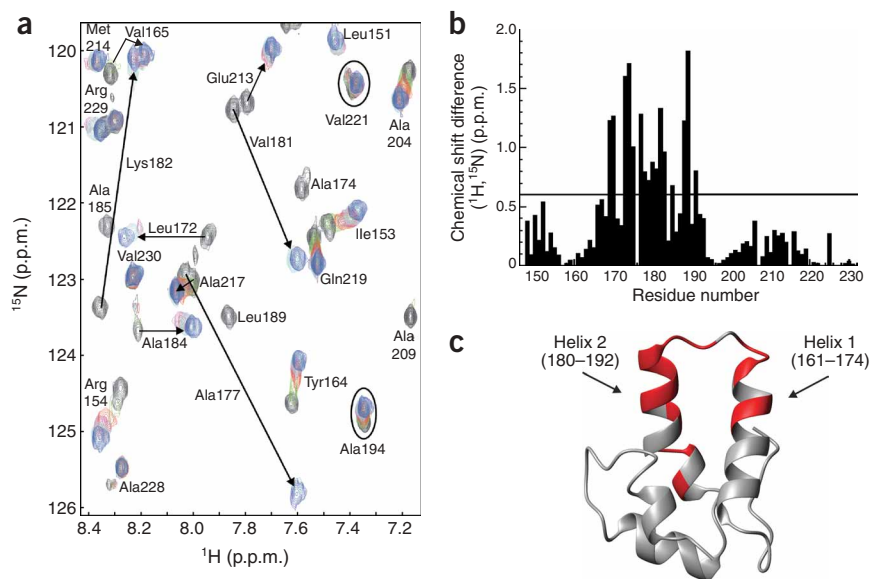
Figure 6 NMR chemical shift perturbation analysis. (**a**) Overlay of a series of 2D ^{1}H-^{15}N–HSQC spectra obtained for the titration of free C-CA$_{W184A/M185A}$ (130 μM, black) with increasing concentrations of CAI (peptide/protein ratio as follows: 0.5:1 (green), 1:1 (red), 2:1 (magenta), 4:1 (cyan), 7.3:1 (blue)). Examples of peaks shifting upon CAI titration are indicated by arrows, and unaffected peaks are circled. For clarity, only part of the spectrum is shown. (**b**) ^{1}H-^{15}N chemical shift perturbations plotted for each assigned amino acid of C-CA$_{W184A/M185A}$ (CA residue numbering). The horizontal line indicates a substantial chemical shift perturbation (0.6 p.p.m.). (**c**) Ribbon diagram of C-CA (ref. 6) generated with MOLMOL[44]. Residues showing chemical shift perturbations >0.06 p.p.m. are colored red. The orientation of the structure was chosen to best visualize the affected residues.

does not substantially reduce C-CA dimerization equilibrium. We also observed that the indole-NH of Trp184 had multiple broad resonances, indicating a dynamic equilibrium of conformers in the dimer interface of both the free and peptide-bound C-CA. This probably also leads to line broadening, resulting in the absence of several backbone-NH resonances of residues in proximity to the dimer interface. Similar observations have been made previously[27]. Accordingly, in solution the dimer interface of C-CA in the free and CAI-bound forms seems to consist of a dynamic ensemble of conformers that interconvert on a microsecond to millisecond timescale.

DISCUSSION
In this study, we identified a previously unknown peptide inhibitor of HIV-1 assembly *in vitro*, CAI. By pointing to the location of a reactive site in the CA protein, this peptide may present a suitable lead compound for antiviral drug development. Peptide inhibitors have inherent drawbacks, as they usually have a short half-life and poor bioavailability; accordingly, we found that neither addition of the peptide to virus-producing cells in culture nor peptide transfection caused any inhibition of HIV-1 release. Thus, CAI cannot be directly used as an antiviral agent, but CAI-CA binding may be used as tool for drug screening and as a starting point for drug design. Furthermore, unraveling the mechanism of assembly inhibition by CAI will shed light on the two-step assembly pathway of HIV and other retroviruses.

A reactive site in CA
The peptides selected by phage display for binding to CA or C-CANC showed a clear preference for a single binding site within C-CA. This was unexpected for a protein that is not designed for interactions of nanomolar affinity and is thus unlikely to have highly active surfaces.

It also implies that the surface of N-CA does not provide high-affinity binding sites for 12-mer peptides present in this library. Selection of a limited number of sequences has been observed in previous phage display experiments using other targets, and it has been suggested that only a limited number of sites on a protein surface are available for interaction[30]. The sequence similarities among group 1 peptides allowed the identification of conserved hydrophobic residues potentially important for interaction with C-CA. In a helical wheel representation of the CAI sequence, these conserved residues form the hydrophobic surface of an amphipathic helix. Although the computationally determined intrinsic helicity of group 1 peptides was negligible, formation of the amphipathic helix is indeed induced upon binding to C-CA, as shown by the crystal structure described in the accompanying paper[23].

The CAI binding site was mapped to the region spanning helices 1 and 2 of C-CA. This result, obtained under physiological conditions in solution, correlates very well with the interaction observed in the accompanying crystal structure of the C-CA–CAI complex[23]. The majority of CA residues interacting with CAI in this structure mapped to amino acids 162–190. Additional contacts involved helix 4 of C-CA, which forms part of the hydrophobic groove that CAI binds to, and which was also identified as part of the binding site in our ELISA experiments. No significant chemical shift perturbations were observed in this region, indicating that side chain interactions mediated by helix 4 do not translate into significant backbone chemical shift perturbation in the context of C-CA$_{W184A/M185A}$.

Mechanism of assembly inhibition by CAI
CAI inhibits assembly of mature- and immature-like particles *in vitro*. Because the ultrastructure of immature viruses and mature conical cores is very similar to those of *in vitro*–assembled spherical and tubular particles, respectively[1,9,14,26], CAI probably targets a region important for both assembly steps. This may reflect an interaction common to the immature Gag shell and the mature capsid; it could also suggest that CAI binding interferes with the essential flexibility of CA by locking it in a conformation incompatible with particle formation. The C-CA subdomain of HIV-1 Gag has been targeted by mutational analyses[10,12,13,31–33], but residues forming the CAI-binding groove have largely been excluded from these studies. Insertion of five amino acids at CA residue 170 abolishes virus release[34], but it is difficult to draw conclusions from such a drastic alteration. Residues Leu172 and Glu187, which interact with CAI in the crystal structure of the complex[23], are part of the C-CA dimer interface[10]. It has previously been suggested that a region including helix 4 of C-CA is involved in assembly: mutation of residues 212–214 abolishes particle release[31], and a peptide covering residues 210–218 inhibits production of infectious particles[17]. However, it has more recently been reported that mutation of the three surface-exposed residues Pro207, Glu212 and Gln219 has no effect on assembly, release or core formation[12]. Recently, an N-CA–C-CA interaction involving residues 55–68 of N-CA

and a region spanning helices 1 and 2 of C-CA has been observed in *in vitro*–assembled tubular particles[11]. The same region of C-CA forms the binding site for CAI, suggesting that the peptide may target this interface. Further analysis has shown, however, that residues 55–68 are protected in the mature capsid but not in immature particles[3], so this interface may only be relevant in the second assembly step. This possibility is supported by studies of the inhibitor CAP-1, which targets the N-CA region involved in this interdomain interaction and specifically inhibits cone formation, but not assembly and release of immature particles[20]. CAI, on the other hand, inhibits assembly of both immature- and mature-like particles *in vitro*. Accordingly, the N-CA–C-CA interaction could explain the inhibition of tubular particles, but it is unlikely to represent the inhibitory mechanism for spherical particles.

Mutation of the CA dimer interface residues Trp184 and Met185 impairs the assembly of immature and mature particles[6,11–13,35] as well as the CAI-CA interaction, suggesting that CAI may inhibit assembly by blocking CA (or Gag) dimerization. The accompanying crystal structure[23] shows that CAI does not directly bind at the dimer interface, and this agrees with the pattern of chemical shift perturbation data. In addition, rotational correlation times show that CAI binding to C-CA does not greatly affect the monomer-dimer equilibrium of C-CA in solution, even though an altered dimer with a markedly reduced buried surface area is observed in the X-ray structure of the C-CA–CAI complex. Hence, it appears more likely that CAI binding leads to formation of a nonfunctional dimer, which either may have lost an essential assembly interface (or different interfaces for immature and mature particle assembly) or may be impossible to incorporate into the particle. The stoichiometry of inhibition suggests that CAI acts in a *trans*-dominant manner, trapping assembly intermediates in a nonfunctional state in addition to binding protein dimers and withdrawing them from the assembly reaction.

A two-step inhibitor

Selection of CAI by phage display screening and characterization of its binding site and mechanism of inhibition defines a new target for antiviral drugs against HIV. The K_d for the interaction of CAI with wild-type CA must be substantially lower than the 15 μM determined for the dimerization-defective variant, as the mutant protein has a lower affinity. The CAI binding site was mapped to a hydrophobic groove that is highly conserved in HIV-1, HIV-2 and SIV (**Fig. 2** of the accompanying paper[23]). Furthermore, CAI integrates the potential of two inhibitors in a single molecule: a drug based on the CAI-CA interaction can be expected to block immature virus assembly in the infected cell and may also target escaping virions by being incorporated into the particle and subsequently blocking the functionally separate formation of the mature capsid. The affinity of the CAI-CA interaction is similar to that between CA and CypA[36], which is also incorporated into virus particles[37]. Furthermore, CAP-1 interferes with HIV maturation despite its low binding affinity (K_d ~800 μM). In summary, CAI is the first inhibitor targeting assembly of immature HIV-1 particles, and a drug based on this peptide could be the first inhibitor with the potential to block virus replication at two consecutive and distinct steps.

METHODS

Proteins and peptides. pET11c plasmids[14,25] coding for Gag-derived proteins (HIV-1NL4-3[38] or HIV-1BH10[39] (ΔMACANCSP2)) were transformed in *Escherichia coli* BL21(DE3) CodonPlus-RIL (Stratagene). CA$_{P207A}$, CA$_{E212A}$ and CA$_{Q219A}$ plasmids were provided by W.I. Sundquist (University of Utah, Salt Lake City, USA); additional CA variants were obtained from pET11c-CA by PCR mutagenesis. Proteins were isotope-labeled in M9 minimal medium

supplemented with 1 g l^{-1} ^{15}N-NH$_4$Cl (CK Gas) and 2 g l^{-1} [^{13}C]glucose (Cambridge Isotope Laboratories). CA, CANC and ΔMACANCSP2 proteins were purified as previously described[14,25]. C-CANC, C-CA and C-CA$_{W184A/M185A}$ were purified by ammonium sulfate precipitation and anion exchange, followed by heparin affinity chromatography (C-CANC) or cation exchange chromatography (C-CA, C-CA$_{W184A/M185A}$) and gel filtration (POROS HQ, HE, HS, PerSeptive Biosystems; Superdex75 HR 10/30, Amersham Biosciences). NC was obtained by proteolytic cleavage of pure C-CANC with recombinant HIV-1 protease (gift from J. Konvalinka, Czech Academy of Sciences, Prague, Czech Republic) followed by HE chromatography.

NMR sample concentrations were 1 mM for 3D experiments and 130 μM for chemical shift perturbation in 100 mM ammonium acetate pH 7.0, 5% D$_2$O, 0.02% (w/v) sodium azide and 2–10 mM Tris(2-carboxyethyl)phosphine (TCEP). Integrity of NMR samples was verified by mass spectrometry. Peptides were obtained as lyophilized trifluoroacetic acid salts (Peptide Specialty Laboratories GmbH). Concentrations were estimated spectrophotometrically using calculated extinction coefficients.

Phage display. An M13 phage library (Ph.D.-12, New England Biolabs) encoding random linear 12-mer peptides at the N-terminus of their pIII coat protein (2.7 × 10^9 sequences) was used. The purified recombinant proteins CA and C-CANC as well as BSA and NC were immobilized on tosyl-activated Dynabeads M-280 (Dynal Biotech) using 12 μg protein per 10^7 beads as recommended.

Dynabeads coated with positive targets were washed with TBSGT (50 mM Tris, pH 7.5, 150 mM NaCl, 0.25% (w/v) gelatin, 0.1% (v/v) Tween 20) and incubated in TBSG at 4 °C with an amount of the phage library equivalent to its 55-fold complexity. Bound phages were eluted with 0.2 M glycine, pH 2.2, 1 mg ml^{-1} BSA and neutralized with 1 M Tris, pH 9.1. Eluates were incubated overnight with Dynabeads coated with negative targets. *E. coli* ER2738 cells were infected with the supernatant and amplified for 4.5 h at 37 °C. Purified phages were used for additional negative and positive selection. Phage DNA was prepared and the region of interest was sequenced with the supplied 96gIII primer.

Enzyme-linked immunosorbent assay of phages. Nunc MaxiSorp ELISA plates were coated overnight with 2 μg ml^{-1} target proteins (CA or BSA in the case of the CA selection and C-CANC or NC in the case of the C-CANC selection), washed with PBS with 0.05% (v/v) Tween 20 (PBST) and blocked with 5% milk powder in PBST for 4 h at room temperature. Plates were incubated overnight at 4 °C with phages amplified from single plaques or purified phages presenting CAI (2.4 × 10^6 PFU μl^{-1} phage-CAI). Bound phages were detected with a monoclonal antibody to M13, conjugated to horseradish peroxidase (Amersham Biosciences, 1:5,000 in blocking buffer). ELISAs were developed using standard procedures. For competition tests with synthetic peptides, phage-CAI (1.2 × 10^6 PFU μl^{-1}) was mixed with final peptide concentrations of 50, 25, 5, 2.5 or 0 μg ml^{-1} before being transferred onto ELISA plates as described above.

***In vitro* assembly and electron micrograph analysis.** *In vitro* assembly was induced by dialysis as previously described[14,25], but reactions were performed in 0.1-kDa-cutoff dialysis tubing (SpectraPor) to retain the peptide. Before dialysis, 25 μM ΔMACANCSP2 or 15 μM CANC was preincubated for 30 min at 4 °C with or without a 0.25-fold–5-fold molar excess of peptide. Assembled particles were pelleted by centrifugation for 5 min at 17,600*g* and resuspended in dialysis buffer in a quarter of the original volume. Next, 6 μl of the resuspended pellets were adsorbed onto glow-discharged carbon-coated copper grids and stained with 2% (w/v) uranyl acetate. For quantification, spherical particles per viewing area were counted at 14,000-fold magnification (20 areas per grid were averaged). CA (117 μM) was preincubated with or without a ten-fold molar excess of peptide in the presence of 1.75% (v/v) DMSO and *in vitro* assembly reactions were started in 0.5 M NaCl.

Nuclear magnetic resonance spectroscopy. NMR spectra of isotope-labeled C-CA and C-CA$_{W184A/M185A}$ were collected at 25 °C on a 600 MHz Varian INOVA spectrometer equipped with a room-temperature probe (Varian). Resonance assignments of the free and peptide-bound forms of the backbone ^{15}N and HN nuclei were obtained by 2D ^{1}H-^{15}N–HSQC, 3D ^{15}N-edited NOESY–HSQC and ^{15}N-edited TOCSY–HSQC, as well as

HNCA, HNCACB and CBCA(CO)NH spectra incorporating water flip-back and gradient enhancement[40,41].

The peptide binding site was obtained by recording a series of eight 2D ^{1}H-^{15}N–HSQC spectra at peptide/protein ratios of 0:1, 0.25:1, 0.5:1, 1:1, 1.5:1, 2:1, 3:1, 4:1 and 7.3:1. K_ds were obtained for residues in the fast-exchange regime by fitting the fractional shift

$$\frac{\Delta}{\Delta_{\max}} = \frac{(K_d + [L] + [P]) - \sqrt{(K_d + [L] + [P])^2 - 4[P][L]}}{2[P]},$$

where $\Delta/\Delta_{\max}$ is the fractional shift and [L] and [P] are the ligand (CAI) and protein (C-CA$_{W184A/M185A}$) concentrations.

The backbone chemical shift perturbation upon peptide addition was calculated by weighting ^{1}HN and ^{15}N chemical shift differences as follows:

$$\Delta\delta = \sqrt{[(\Delta\delta_H)^2 + 1/6(\Delta\delta_N)^2]},$$

where $\Delta\delta_H$ and $\Delta\delta_N$ are the differences between the HN and ^{15}N chemical shifts, respectively, of the fully saturated and free protein.

Rotational correlation times were determined from the ratios of the average ^{15}N-T_1 and ^{15}N-T_2 relaxation time constants. ^{15}N–C-CA was analyzed at a concentration of 0.1–1 mM either free or saturated to more than 95% with CAI. T_1 and T_2 values were obtained by exponential fits to the measured intensity decays of a series of 2D ^{1}H-^{15}N–T_1/T_2, measurements with delay times of 0.02, 0.08, 0.16, 0.32, 0.6, 1.0 and 1.4 s for T_1 and 0.01, 0.03, 0.05, 0.07, 0.11 and 0.15 s for T_2.

All NMR data were processed with NMRPipe[42], using mild resolution enhancement and linear prediction in the heteronuclear dimension, before being subjected to Fourier transformation. The resulting spectra were analyzed with NMRView[43].

Accession codes. BIND identifier (http://bind.ca): 300896.

COMPETING INTERESTS STATEMENT
The authors declare that they have no competing financial interests.

1. Briggs, J.A. *et al.* The stoichiometry of Gag protein in HIV-1. *Nat. Struct. Mol. Biol.* **11**, 672–675 (2004).
2. Wiegers, K. *et al.* Sequential steps in human immunodeficiency virus particle maturation revealed by alterations of individual Gag polyprotein cleavage sites. *J. Virol.* **72**, 2846–2854 (1998).
3. Lanman, J. *et al.* Key interactions in HIV-1 maturation identified by hydrogen-deuterium exchange. *Nat. Struct. Mol. Biol.* **11**, 676–677 (2004).
4. Accola, M.A., Höglund, S. & Göttlinger, H.G. A putative alpha-helical structure which overlaps the capsid-p2 boundary in the human immunodeficiency virus type 1 Gag precursor is crucial for viral particle assembly. *J. Virol.* **72**, 2072–2078 (1998).
5. Gitti, R.K. *et al.* Structure of the amino-terminal core domain of the HIV-1 capsid protein. *Science* **273**, 231–235 (1996).
6. Gamble, T.R. *et al.* Structure of the carboxyl-terminal dimerization domain of the HIV-1 capsid protein. *Science* **278**, 849–852 (1997).
7. Worthylake, D.K., Wang, H., Yoo, S., Sundquist, W.I. & Hill, C.P. Structures of the HIV-1 capsid protein dimerization domain at 2.6Å resolution. *Acta Crystallogr. D Biol. Crystallogr.* **55**, 85–92 (1999).
8. Mortuza, G.B. *et al.* High-resolution structure of a retroviral capsid hexameric amino-terminal domain. *Nature* **431**, 481–485 (2004).
9. Li, S., Hill, C., Sundquist, W. & Finch, J. Image reconstructions of helical assemblies of the HIV-1 CA protein. *Nature* **407**, 409–413 (2000).
10. del Álamo, M., Neira, J.L. & Mateu, M.G. Thermodynamic dissection of a low affinity protein-protein interface involved in human immunodeficiency virus assembly. *J. Biol. Chem.* **278**, 27923–27929 (2003).
11. Lanman, J. *et al.* Identification of novel interactions in HIV-1 capsid protein assembly by high-resolution mass spectrometry. *J. Mol. Biol.* **325**, 759–772 (2003).
12. von Schwedler, U.K., Stray, K.M., Garrus, J.E. & Sundquist, W.I. Functional surfaces of the human immunodeficiency virus type 1 capsid protein. *J. Virol.* **77**, 5439–5450 (2003).
13. Ganser-Pornillos, B.K., von Schwedler, U.K., Stray, K.M., Aiken, C. & Sundquist, W.I. Assembly properties of the human immunodeficiency virus type 1 CA protein. *J. Virol.* **78**, 2545–2552 (2004).
14. Gross, I. *et al.* A conformational switch controlling HIV-1 morphogenesis. *EMBO J.* **19**, 103–113 (2000).
15. Campbell, S. *et al.* Modulation of HIV-like particle assembly *in vitro* by inositol phosphates. *Proc. Natl. Acad. Sci. USA* **98**, 10875–10879 (2001).
16. Ivanov, D., Stone, J.R., Maki, J.L., Collins, T. & Wagner, G. Mammalian SCAN domain dimer is a domain-swapped homolog of the HIV capsid C-terminal domain. *Mol. Cell* **17**, 137–143 (2005).
17. Niedrig, M. *et al.* Inhibition of infectious human immunodeficiency virus type 1 particle formation by Gag protein-derived peptides. *J. Gen. Virol.* **75**, 1469–1474 (1994).
18. Höglund, S. *et al.* Tripeptide interference with human immunodeficiency virus type 1 morphogenesis. *Antimicrob. Agents Chemother.* **46**, 3597–3605 (2002).
19. Garzón, M.T. *et al.* The dimerization domain of the HIV-1 capsid protein binds a capsid protein-derived peptide: a biophysical characterization. *Protein Sci.* **13**, 1512–1523 (2004).
20. Tang, C. *et al.* Antiviral inhibition of the HIV-1 capsid protein. *J. Mol. Biol.* **327**, 1013–1020 (2003).
21. Li, F. *et al.* PA-457: a potent HIV inhibitor that disrupts core condensation by targeting a late step in Gag processing. *Proc. Natl. Acad. Sci. USA* **100**, 13555–13560 (2003).
22. Zhou, J. *et al.* Small-molecule inhibition of human immunodeficiency virus type 1 replication by specific targeting of the final step of virion maturation. *J. Virol.* **78**, 922–929 (2004).
23. Ternois, F., Sticht, J., Duquerroy, S., Kräusslich, H.-G. & Rey, A.F. Crystal structure of the HIV-1 capsid protein C-terminal domain in complex with an inhibitor of particle assembly. *Nat. Struct. Mol. Biol.* **12**, 678–682 (2005).
24. Kräusslich, H.-G., Fäcke, M., Heuser, A.M., Konvalinka, J. & Zentgraf, H. The spacer peptide between human immunodeficiency virus capsid and nucleocapsid proteins is essential for ordered assembly and viral infectivity. *J. Virol.* **69**, 3407–3419 (1995).
25. Gross, I., Hohenberg, H. & Kräusslich, H. In vitro assembly properties of purified bacterially expressed capsid proteins of human immunodeficiency virus. *Eur. J. Biochem.* **249**, 592–600 (1997).
26. Briggs, J.A.G., Wilk, T., Welker, R., Kräusslich, H.-G. & Fuller, S.D. Structural organization of authentic, mature HIV-1 virions and cores. *EMBO J.* **22**, 1707–1715 (2003).
27. Newman, J.L., Butcher, E.W., Patel, D.T., Mikhaylenko, Y. & Summers, M.F. Flexibility in the P2 domain of the HIV-1 Gag polyprotein. *Protein Sci.* **13**, 2101–2107 (2004).
28. Lanman, J., Sexton, J., Sakalian, M. & Prevelige, P. Kinetic analysis of the role of intersubunit interactions in human immunodeficiency virus type 1 capsid protein assembly in vitro. *J. Virol.* **76**, 6900–6908 (2002).
29. Mateu, M.G. Conformational stability of dimeric and monomeric forms of the C-terminal domain of human immunodeficiency virus-1 capsid protein. *J. Mol. Biol.* **318**, 519–531 (2002).
30. Hyde-DeRuyscher, R. *et al.* Detection of small-molecule enzyme inhibitors with peptides isolated from phage-displayed combinatorial peptide libraries. *Chem. Biol.* **7**, 17–25 (2000).
31. Kattenbeck, B., von Poblotzki, A., Rohrhofer, A., Wolf, H. & Modrow, S. Inhibition of human immunodeficiency virus type 1 particle formation by alterations of defined amino acids within the C terminus of the capsid protein. *J. Gen. Virol.* **78**, 2489–2496 (1997).
32. Forshey, B.M., von Schwedler, U., Sundquist, W.I. & Aiken, C. Formation of a human immunodeficiency virus type 1 core of optimal stability is crucial for viral replication. *J. Virol.* **76**, 5667–5677 (2002).
33. Liang, C., Hu, J., Whitney, J.B., Kleiman, L. & Wainberg, M.A. A structurally disordered region at the C terminus of capsid plays essential roles in multimerization and membrane binding of the gag protein of human immunodeficiency virus type 1. *J. Virol.* **77**, 1772–1783 (2003).
34. Reicin, A.S. *et al.* Linker insertion mutations in the human immunodeficiency virus type 1 *gag* gene: effects on virion particle assembly, release, and infectivity. *J. Virol.* **69**, 642–650 (1995).
35. von Schwedler, U.K. *et al.* Proteolytic refolding of the HIV-1 capsid protein amino-terminus facilitates viral core assembly. *EMBO J.* **17**, 1555–1568 (1998).
36. Yoo, S. *et al.* Molecular recognition in the HIV-1 capsid/cyclophilin A complex. *J. Mol. Biol.* **269**, 780–795 (1997).
37. Franke, E.K., Yuan, H.E. & Luban, J. Specific incorporation of cyclophilin A into HIV-1 virions. *Nature* **372**, 359–362 (1994).
38. Adachi, A. *et al.* Production of acquired immunodeficiency syndrome-associated retrovirus in human and nonhuman cells transfected with an infectious molecular clone. *J. Virol.* **59**, 284–291 (1986).
39. Ratner, L. *et al.* Complete nucleotide sequences of functional clones of the AIDS virus. *AIDS Res. Hum. Retroviruses* **3**, 57–69 (1987).
40. Kay, L.E. Pulsed-field gradient multidimensional NMR methods for the study of protein structure and dynamics. *Prog. Biophys. Mol. Biol.* **63**, 277–299 (1995).
41. Sattler, M., Schleucher, J. & Griesinger, C. Heteronuclear multidimensional NMR experiments for the structure determination of proteins in solution employing pulsed field gradients. *Prog. Nucl. Magn. Reson. Spectrosc.* **34**, 93–158 (1999).
42. Delaglio, F. *et al.* NMRPipe: a multidimensional spectral processing system based on UNIX pipes. *J. Biomol. NMR* **6**, 277–293 (1995).
43. Johnson, B.A. & Blevins, R.A. NMRView: a computer program for the visualization and analysis of NMR data. *J. Biomol. NMR* **4**, 603–614 (1994).
44. Koradi, R., Billeter, M. & Wüthrich, K. MOLMOL: a program for display and analysis of macromolecular structure. *J. Mol. Graph.* **14**, 51–55 (1996).